INSTITUTE OF PHYSICS PUBLISHING and INTERNATIONAL ATOMIC ENERGY AGENCY NUCLEAR FUSION

Nucl. Fusion **46** (2006) 635–644 doi:10.1088/0029-5515/46/5/014

Resistive wall stabilized operation in rotating high beta NSTX plasmas

S.A. Sabbagh[1], A.C. Sontag[1], J.M. Bialek[1], D.A. Gates[2], A.H. Glasser[3], J.E. Menard[2], W. Zhu[1], M.G. Bell[2], R.E. Bell[2], A. Bondeson[4], C.E. Bush[5], J.D. Callen[6], M.S. Chu[7], C.C. Hegna[6], S.M. Kaye[2], L.L. Lao[7], B.P. LeBlanc[2], Y.Q. Liu[4], R. Maingi[5], D. Mueller[2], K.C. Shaing[6], D. Stutman[8], K. Tritz[8] and C. Zhang[9]

[1] Department of Applied Physics and Applied Mathematics, Columbia University, New York, NY, USA
[2] Princeton Plasma Physics Laboratory, Princeton University, Princeton, NJ, USA
[3] Los Alamos National Laboratory, Los Alamos, NM, USA
[4] Department of Applied Mechanics, Chalmers University of Technology, Gothenburg, Sweden
[5] Oak Ridge National Laboratory, Oak Ridge, TN, USA
[6] University of Wisconsin, Madison, WI, USA
[7] General Atomics, San Diego, CA, USA
[8] Johns Hopkins University, Baltimore, MD, USA
[9] Institute of Plasma Physics, Chinese Academy of Sciences, Hefei, China

E-mail: sabbagh@pppl.gov

Received 9 September 2005, accepted for publication 3 April 2006
Published 28 April 2006
Online at stacks.iop.org/NF/46/635

Abstract

The National Spherical Torus Experiment (NSTX) has demonstrated the advantages of low aspect ratio geometry in accessing high toroidal and normalized plasma beta, $\beta_t \equiv 2\mu_0\langle p\rangle/B_0^2$ and $\beta_N \equiv 10^8\langle\beta_t\rangle aB_0/I_p$. Experiments have reached $\beta_t = 39\%$ and $\beta_N = 7.2$ through boundary and profile optimization. High β_N plasmas can exceed the ideal no-wall stability limit, $\beta_{N\text{no-wall}}$, for periods much greater than the wall eddy current decay time. Resistive wall mode (RWM) physics is studied to understand mode stabilization in these plasmas. The toroidal mode spectrum of unstable RWMs has been measured with mode number n up to 3. The critical rotation frequency of Bondeson–Chu, $\Omega_{crit} = \omega_A/(4q^2)$, describes well the RWM stability of NSTX plasmas when applied over the entire rotation profile and in conjunction with the ideal stability criterion. Rotation damping and global rotation collapse observed in plasmas exceeding $\beta_{N\text{no-wall}}$ differs from the damping observed during tearing mode activity and can be described qualitatively by drag due to neoclassical toroidal viscosity in the helically perturbed field of an ideal displacement. Resonant field amplification of an applied $n = 1$ field perturbation has been measured and increases with increasing β_N. Equilibria are reconstructed including measured ion and electron pressure, toroidal rotation and flux isotherm constraint in plasmas with core rotation ω_ϕ/ω_A up to 0.48. Peak pressure shifts of 18% of the minor radius from the magnetic axis have been reconstructed.

PACS numbers: 52.55.Fa, 52.55.Tn, 52.35.Py, 52.65.Kj

(Some figures in this article are in colour only in the electronic version)

1. Introduction

Stabilizing modes that limit plasma beta is a key goal in fusion reactor design. The National Spherical Torus Experiment (NSTX) [1] has demonstrated the advantages of low aspect ratio geometry in accessing high toroidal and normalized plasma beta $\beta_t \equiv 2\mu_0\langle p\rangle/B_0^2$ and $\beta_N \equiv 10^8\langle\beta_t\rangle aB_0/I_p$, where p is the plasma pressure, B_0 is the vacuum toroidal field at the plasma geometric centre, a is the plasma minor radius at the midplane, I_p is the plasma current and brackets represent volume average. Plasmas have reached $\beta_t = 39\%$ and $\beta_N = 7.2$ through boundary and profile optimization [2]. ST devices normally achieve higher β_N than devices with higher aspect ratio and the present result represents the highest β_N yet achieved in the ST.

Global magnetohydrodynamic (MHD) instabilities are observed to limit beta in NSTX plasmas. Plasmas with the highest β_N exceed the ideal no-wall MHD stability limit by

passive stabilization of the external kink/ballooning instability through the combination of sufficiently rapid plasma rotation and the presence of nearby electrically conducting plates and vacuum vessel [3–5]. However below a critical rotation frequency, $\Omega_{\rm crit}$, the resistive wall mode (RWM), a kink mode modified by the presence of the conducting wall, can become unstable and grow, leading to rapid rotation damping and beta collapse on the wall eddy current decay time [6–8]. The RWM has a growth rate and real frequency $\sim O(1/\tau_w) \sim 100$ Hz in NSTX. Understanding the unstable mode spectrum, the physics of instability-induced rotation damping, the critical rotation frequency for mode stabilization and developing methods for active feedback control of the RWM have general application for optimizing toroidal magnetic confinement systems including advanced operational scenarios in ITER. Large scale resistive plasma tearing modes also limit beta and reduce plasma rotation but on a timescale typically longer than τ_w [9]. These modes can have growth rates similar to the RWM but have measured frequencies nearly equal to the plasma rotation frequency, ω_ϕ, in the region of the island. Typically in NSTX, $\omega_\phi/2\pi \sim 10$ kHz in neutral beam heated plasmas. The ideal kink/RWM perturbation can also trigger pure toroidal mode number $n = 1$–3 tearing modes [10]. Tearing modes typically saturate and cause a soft beta limit, while unstable RWMs grow to a large amplitude and cause rapid and significant beta collapses or disruptions.

The present work focuses on wall stabilization physics of kink/RWM instabilities in high beta ST plasmas. Extensive research has been conducted on the RWM and the mode has been successfully stabilized for times significantly exceeding both τ_w and the energy confinement time, τ_E [10–12]. Study has focused on the RWM with $n = 1$ as it is typically the least stable RWM in tokamaks since it minimizes the field line bending of the dominant toroidal field. Theoretical calculations show that high beta ST plasmas, where the vacuum toroidal field is significantly lower, allow $n = 2$ and higher modes to be unstable at β_N values close to the value at which the $n = 1$ mode becomes unstable [10, 13]. Research on the higher-n instabilities is important for the development of systems to stabilize these modes with the goal of sustaining operation at the highest plasma beta. The Fitzpatrick–Aydemir (F–A) model [14,15] of the RWM is referenced throughout this work to compare experimental observations with theory. The theory uses cylindrical geometry with an axial field variation chosen to model the tokamak toroidal field. The RWM is taken as primarily an external mode, with plasma dynamics limited to a thin inertial layer near the plasma edge. Although simplified, this model does well to qualitatively represent general RWM dynamics in NSTX, such as mode rotation, that are not characteristically altered by plasma aspect ratio or elongation. It has been used successfully to model timescales of RWM response to error field alteration in HBT-EP [16].

In section 2, the operational space of wall-stabilized, high beta plasmas is examined, along with discharge dynamics and margins over ideal MHD stability limits. Section 3 examines in detail the RWM dynamics and toroidal mode spectrum observed. Section 4 illustrates the importance of plasma rotation on stabilizing the RWM and how the mode itself reduces this stabilizing rotation. The critical plasma rotation frequency for stabilization of the RWM is examined as a function of safety factor profile and compared with theory. The plasma rotation damping caused by the RWM is measured and is well explained by drag due to neoclassical toroidal viscosity (NTV). The high beta plasma response to non-rotating, non-axisymmetric applied fields is described in section 5. The effect of the rapid plasma rotation of the reconstructed equilibria is analysed in section 6. Conclusions are given in section 7.

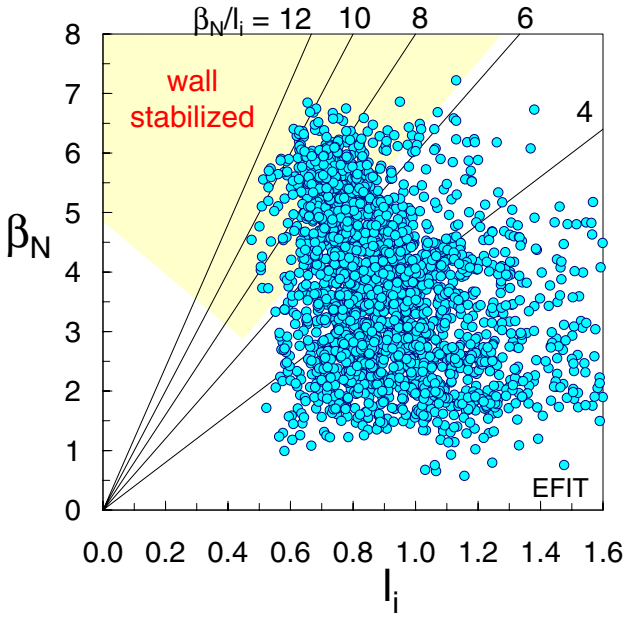

Figure 1. NSTX operational space plotted as β_N versus l_i.

2. High beta plasmas and stability limits

Stability research on tokamaks has yielded an empirical scaling for the maximum achievable β_N that linearly increases with the plasma internal inductance, l_i, and the stability of ideal kink and ballooning modes has also been shown to follow such a scaling [17]. For NSTX, the ideal no-wall MHD limit, $\beta_{N\text{no-wall}}$, is roughly approximated by $6l_i$, but it also depends strongly on the pressure profile peaking factor [10]. High β_N plasmas in NSTX routinely exceed $\beta_{N\text{no-wall}}$, reaching high ratios of β_N/l_i of 11, as illustrated in figure 1, where the experimentally achieved β_N is plotted against l_i. At high β_N/l_i ratio, in a limited range of l_i between 0.5 and 0.7, the data may indicate an increasing dependence of the maximum with increasing l_i, but over the wider range of l_i, there is no such dependence. The shaded region in figure 1 generally indicates plasmas that are wall stabilized. Exact calculation of the ideal MHD stability evolution for a plasma discharge is routinely computed as desired by the DCON [18] code using experimental time-evolving equilibrium reconstructions as input. Plasmas with high β_N exceed the ideal no-wall MHD limit and can remain passively stabilized by plasma rotation with $\beta_N/\beta_{N\text{no-wall}} > 1.5$ for periods greatly exceeding the wall eddy current decay time, τ_w. This is illustrated in figure 2, where the evolution of β_N and the core plasma rotation is shown, along with the DCON computed no-wall and with-wall stability criteria, expressed by the parameter, δW. Negative δW indicates violation of the

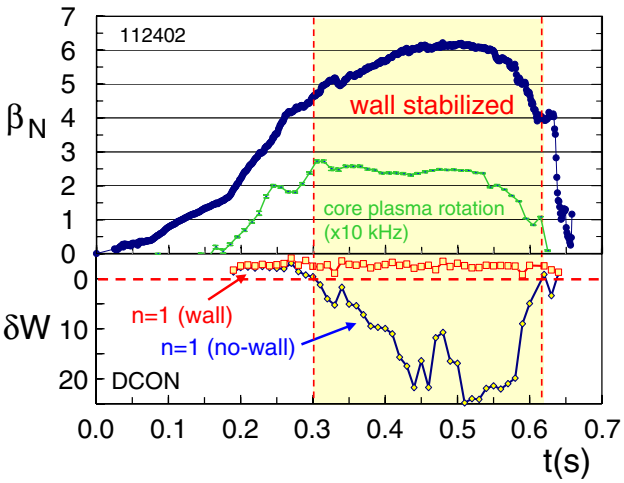

Figure 2. Wall stabilized plasma operation with $\beta_N > \beta_{Nno\text{-}wall}$ at sufficient plasma rotation. The evolution of the no-wall and with-wall stability criteria computed by DCON is shown. The $\beta_N = \beta_{Nno\text{-}wall}$ at a value of 4.6 during the beta increase.

stability limit. The plasma exceeds $\beta_{Nno\text{-}wall}$ when β_N reaches 4.6 and maintains this condition for about $50\tau_w$. Toroidal rotation collapse typically correlates with reduction of β_N from the peak value. In this particular case, saturated tearing modes apparently lead to the slow reduction in core plasma rotation.

3. RWM spectrum and dynamics

NSTX has a major radius, $R = 0.86$ m, aspect ratio $A > 1.27$, I_p up to 1.5 MA and B_0 up to 0.6 T. An array of magnetic field sensors allows the measurement of low frequency MHD modes with $n > 1$. The device is equipped with 48 toroidally segmented copper stabilizer plates, covered with carbon tiles comprising the plasma facing components. These segments are arranged symmetrically in four toroidal rings, two above and two below the device midplane. The plates are independently connected to the stainless steel vacuum vessel by high resistance supports. Magnetic loops measuring the radial, B_r, and poloidal, B_p, flux are located at each of the plates closest to the midplane, the B_r sensors mounted between the carbon tiles and the copper shells and the B_p sensors mounted a few centimetres below each plate. The sensors are instrumented to detect modes with frequencies up to 2.5 kHz.

Unstable RWMs with $n = 1$–3 have been observed in high beta NSTX plasmas. The mode spectrum and dynamics for discharges showing pure mode growth and mode rotation during growth are shown in figure 3. Mode growth and associated beta collapse occur in a few τ_w (about 5 ms). The B_p sensor array shows nearly simultaneous growth of $n = 1$–3 modes in figure 3(*a*) at a peak $\beta_t = 35\%$ and the measured toroidal phases ($n = 1$ phase, ϕ_{B_p}, is shown) do not show mode rotation. RWM dynamics from F–A theory indicate that the mode may rotate as the plasma becomes unstable dependent upon the proximity of the equilibrium to marginal stability. This rotation is observed in the plasma shown in figure 3(*b*). As expected by the F–A theory, the measured mode rotation frequency of 120 Hz is $\sim O(1/\tau_w)$ and the mode phase propagation is in the direction of plasma rotation. At this relatively slow rate, the mode significantly slips behind the measured edge plasma rotation frequency of 2 kHz. This is characteristic of an ideal RWM and differs from a tearing mode perturbation that is theoretically expected to closely match the plasma rotation frequency at the island separatrix. The phase velocity changes in time as the mode rotates through the toroidal location of maximum error field, also expected by F–A theory and illustrated in [15]. An $n = 1$ locked mode detector outside the vacuum vessel begins to measure the RWM about τ_w after it is observed on the B_p sensors due to mode penetration of the vessel; it measures a factor of five less signal and is not capable of detecting the detailed phase shift during RWM growth. Odd-n tearing modes with frequency less than 40 kHz are absent. A full spectrum analysis shows a rapidly rotating (20 kHz) $n = 2$ mode throughout the high beta phase, which is easily distinguished from the RWM.

Time-evolved ideal MHD stability assuming no stabilizing wall for $n = 1$–3 modes was computed for these plasmas with DCON using EFIT [5, 19] equilibrium reconstructions. figures 3(*a*) and (*b*) show that before RWM mode growth, both plasmas exceed the computed $n = 1$–3 ideal no-wall beta limit. Equilibrium variations were considered for the stability calculations by varying the minimum q between 1.1 and 1.7; the $n = 1$–3 modes remained unstable for equilibria approaching the time of RWM growth. Fast camera images confirm the toroidal asymmetry and macroscopic scale of the mode. Moving pictures of these images also show mode rotation in some instances. Visible light emission (figure 4(*a*)) from the plasma shown in figure 3(*a*) is compared with the DCON computed perturbed magnetic field normal to the surface in figures 4(*b*) and (*c*). The computation uses an EFIT experimental equilibrium reconstruction and the illustration includes the sum of the $n = 1$–3 components scaled to the measured RWM sensor amplitudes and relative phases. The perturbed field amplitude shown has been scaled up by a factor of 10 to clarify the mode shape. Based on the measured field amplitudes for $n = 1$–3, an estimate of the real space displacement of the mode is about 3 cm at the outboard midplane. This is consistent with estimates of the mode amplitude based on the fast visible light camera images and electron temperature measurements from past experiments using non-standard relative timing of the two independent lasers used by the Thomson scattering diagnostic [10].

Soft x-ray (SXR) emission measured at two toroidal positions 90° apart shows that the RWM is not localized to a narrow edge region, as assumed by the F–A theory. Figure 5 shows the measured toroidal asymmetry of the SXR emission during RWM growth. In this particular plasma, the mode is not apparent in the core ($R = 1.18$ m, normalized poloidal flux $\psi_n \sim 0.13$) but appears in the channel at $R = 1.31$ m ($\psi_n \sim 0.4$). SXR channels with sightlines at $\psi_n > 0.4$ were not available. The change in electron temperature, T_e, measured by the midplane Thomson scattering diagnostic for similar RWM plasmas shows the perturbation to be maximum at about 1.3 m and much smaller in the plasma core. The theoretical (DCON) $n = 1$ ideal MHD mode decomposition into poloidal harmonics, m, is shown as a function of ψ_n in figure 6(*a*) for the equilibrium shown in figure 5. The three dashed lines indicate the position of the SXR chords. This computation, typically used to determine the structure

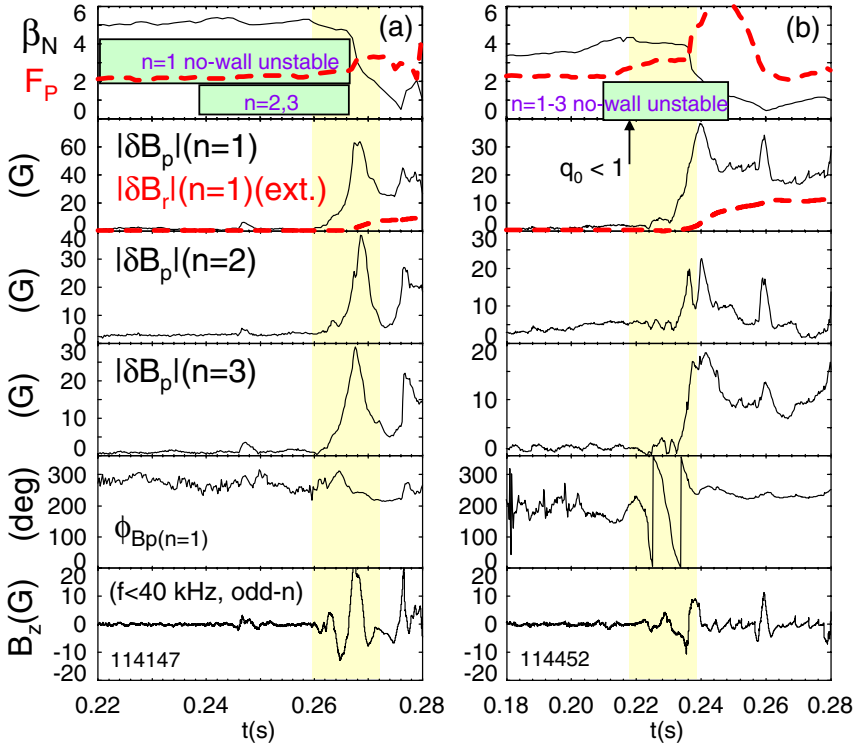

Figure 3. RWM toroidal mode spectrum and dynamics for (*a*) pure growth and (*b*) mode rotation during growth. The evolution of β_N, pressure peaking factor, F_p (- - - -), amplitude of $n = 1$–3 components of mode-generated B_p (internal to vacuum vessel), $n = 1$ B_r (external to vacuum vessel; - - - -), phase of $n = 1$ mode-generated B_p and integrated pickup loop data measuring the vertical field, B_z, for odd-n MHD modes are shown. The computed ideal MHD no-wall stability for $n = 1$–3 is also shown.

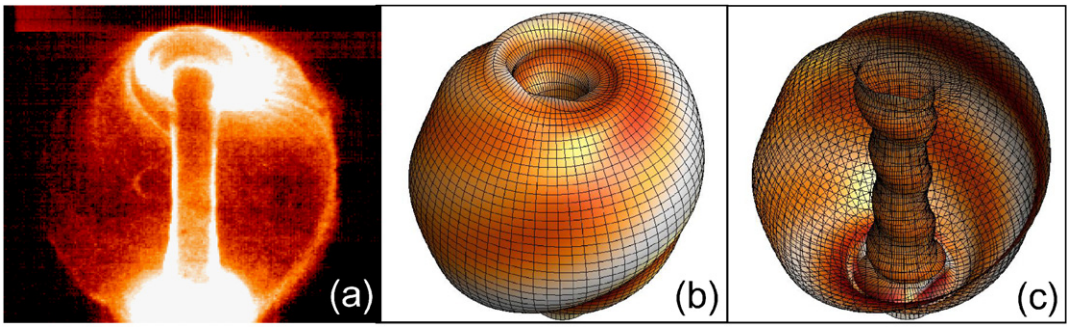

Figure 4. Visible light emission (*a*) and DCON computed normal perturbed field (*b*) and (*c*) for the unstable RWM shown in figure 3(*a*). (discharge 114147) at $t = 0.268$ s.

of the RWM, shows the mode to have global extent and is dominated by the $m = 2$ component at the position where the SXR emission perturbation is the largest. Figure 6(*b*) shows the poloidal variation of the mode field perturbation at the plasma edge. Here, the poloidal angle θ is 0 at the outboard midplane and π at the inboard midplane. The mode has a strong ballooning character being significantly larger on the outboard portion of the plasma.

4. Wall stabilization physics

Sustaining $\beta_N > \beta_{Nno\text{-}wall}$ for periods significantly longer than the RWM growth time requires mode stabilization. Plasma rotation frequencies normalized to the Alfvén frequency, ω_ϕ/ω_A, of a few per cent relative to the mode rotation frequency can passively stabilize the RWM in theory. This has been confirmed experimentally. The ratio of ω_ϕ/ω_A is typically measured at the dominant rational surface (e.g. $q = 2$ in DIII-D) [4]. Previous NSTX research reported a possible decrease in Ω_{crit} with increasing q [10]. Considering Ω_{crit} as a profile, rather than a scalar, plasmas operating at high $\beta_N > \beta_{Nno\text{-}wall}$ for long-pulses in NSTX [20] have toroidal rotation frequency profiles greater than $\Omega_{crit}(q)$. The critical rotation frequency of Bondeson and Chu [21], $\Omega_{crit} = \omega_A/(Cq^2)$ with $C = 4$, well describes RWM stability in conjunction with the ideal stability criterion when applied over the entire rotation profile. This is shown in figure 7, where ω_ϕ/ω_A is plotted versus q at each radial position (51 channels) and time when ω_ϕ is measured for two classes of discharges analysed for ideal $n = 1$ stability with DCON using time-evolved EFIT equilibrium reconstructions. In the discharges described by triangles, ω_ϕ/ω_A never greatly exceeds $1/(4q^2)$. These plasmas do

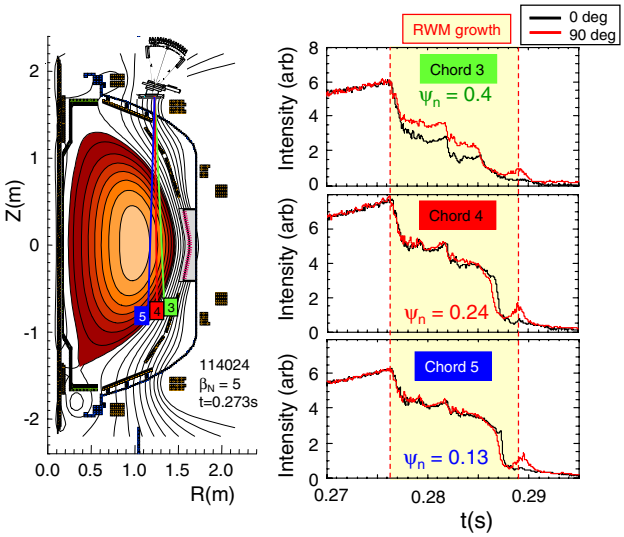

Figure 5. Toroidal asymmetry of measured SXR emission during RWM growth.

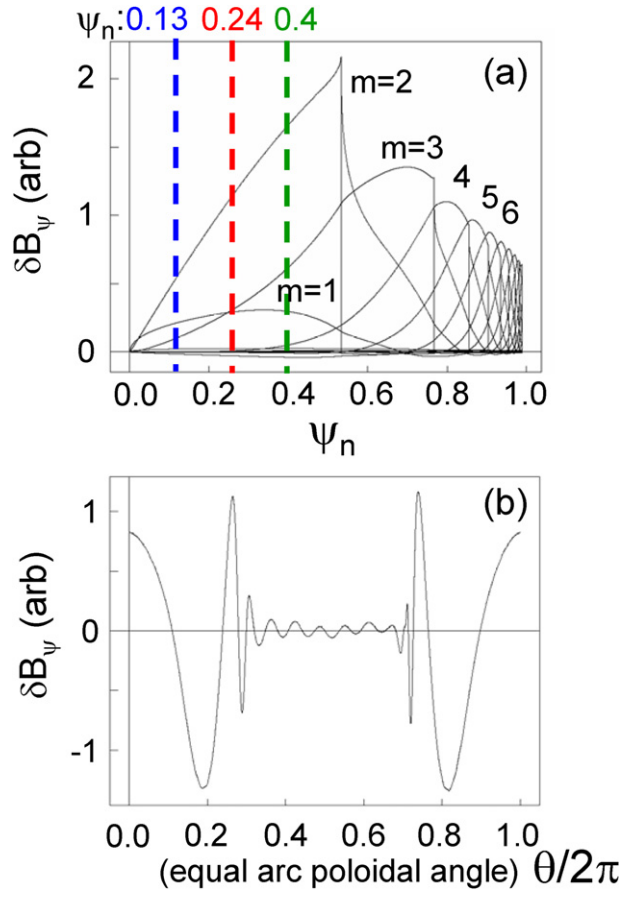

Figure 6. Theoretical computed $n = 1$ ideal mode field normal to the flux surface decomposed into poloidal harmonics as a function of normalized poloidal flux (frame (*a*)) and poloidal variation of the $n = 1$ RWM field at the plasma boundary as a function of poloidal angle (frame (*b*)).

not sustain $\beta_N > \beta_{Nno\text{-}wall}$ for longer than a few τ_w (e.g. discharge 107636 in [10]) without suffering a beta collapse that restores ideal stability. In contrast, plasmas described by plusses maintain $\beta_N > \beta_{Nno\text{-}wall}$ (about 4.8 in these plasmas) at each time point shown for significantly longer than a few τ_w. In these plasmas, the ω_ϕ/ω_A profile always exceeds $1/4q^2$. Plasma rotation and dissipation from ion Landau damping have been linked to RWM stabilization. However, drift-kinetic theory indicates that trapped particle effects strongly reduce ion Landau damping and increase the Pfirsch–Schlüter toroidal inertia enhancement in the RWM range of frequencies [21]. The relative importance of inertia over dissipation is consistent with the observed RWM stabilization at increased q in NSTX. High β_N plasmas can be stabilized with a portion of the ω_ϕ/ω_A profile below $1/4q^2$, but beta collapses can result if this occurs at low-order rational surfaces. While the Bondeson–Chu theory considers finite aspect ratio effects, simplifications are made in the model that might lead one to expect that the constant C might differ between theory and experiment. While the match between experiment and theory is not exact, it is apparently fortuitous that the critical rotation profile found in these experiments is described well by using the Bondeson–Chu value of C.

The standard F–A theory yields a scaling of $\Omega_{crit} \sim 1/q$, rather than $1/q^2$, as shown in the work of Bondeson–Chu. The former does not match NSTX data as well as the latter. One might expect that the difference could be due to the assumed localization of the inertial layer for RWM dynamics to the plasma edge in the F–A theory, whereas for NSTX this is computed to be about the outer 10% of the poloidal flux. However, even if we examine $\Omega_{crit}(q = q_{95})$, within the F–A inertial layer, measurements still support the Bondeson–Chu scaling (figure 7(*b*)). The F–A model can reproduce this scaling if neoclassical viscosity is used [22]. The application of neoclassical viscosity enhances the toroidal inertia thereby lowering the effective Alfvén frequency and reducing Ω_{crit} by an additional factor of $1/q$ compared with the standard F–A result using classical perpendicular inertia.

Rotation damping in plasmas below $\beta_{Nno\text{-}wall}$ can be described by electromagnetic drag due to small magnetic islands and associated viscous plasma coupling [23]. Large-scale MHD modes, especially the 1/1 internal mode and the RWM in NSTX, can cause rapid rotation damping. Understanding the rotation damping physics of these modes is important for sustaining passive stabilization. The large enhancement of rotation damping and consequent global rotation collapse observed during RWM growth (figures 8(*a*) and (*b*)) can be described by non-resonant drag due to NTV caused by the helically perturbed field of the mode [24, 25]. By associating the magnitude of the perturbed field to the measured δT_e, NTV calculations show qualitative agreement between theory and experiment (figure 8(*c*)). In the figure, the experimentally measured plasma rotation damping is expressed as $-\rho R_0^2(d\Omega_\phi/dt)$, where ρ is the plasma mass density, R_0 is the flux surface major radius and T_{NTV} is the theoretical flux surface integrated torque divided by the flux surface volume. The NTV damping torque, that depends on the field perturbation and ion temperature as $\delta B^2 T_i^{0.5}$, appears to explain the lack of damping and sustained plasma rotation of 2 kHz observed at the plasma edge where T_i is small. Note that since δT_e is used in lieu of the perturbed magnetic field in the calculation, T_{NTV} is scaled, and the comparison to the measured rotation damping is qualitative. The dynamics of the rotation damping shows the entire rotation profile decreasing in a self-similar fashion (figure 8(*a*)). This rotation profile evolution

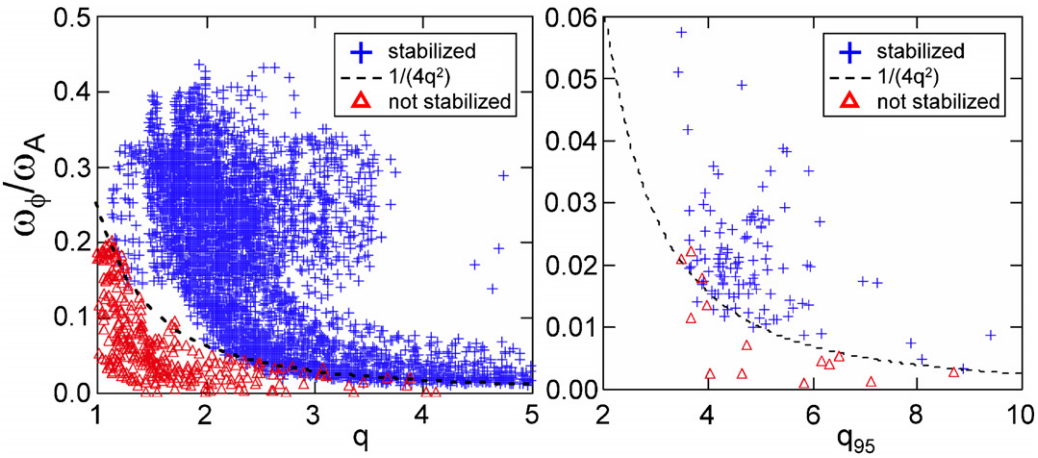

Figure 7. Observed kink/RWM stability versus local ω_ϕ/ω_A, parametrized by local q value (frame (a)) and q_{95} (frame (b)). Ω_{crit} is well defined by the Bondeson–Chu expression $\omega_A/(4q^2)$.

is unlike that caused by damping due to islands, which show a clear radially outward momentum transfer across dominant resonant surfaces (figure 9). Low frequency tearing modes were intentionally avoided during the rotation collapses caused by RWMs shown in figure 8 to clarify the cause of the rotation damping. Further details of the rotation damping profile and the success of NTV theory in explaining the rotation damping due to the 1/1 internal mode are examined in [9].

5. Plasma response to non-axisymmetric fields

The first two coils, of an eventual six to be used for active stabilization of the RWM, have been used to study resonant field amplification (RFA) [26, 27] and to slow rotation below Ω_{crit} by generating $n = 1$ standing wave field perturbations. The coils are external but closely fitted to the vacuum vessel, are diametrically opposed and each cover approximately 60° of toroidal angle. The coils were designed using the VALEN 3D electromagnetic code [28] and are located between the upper and lower primary passive stabilizing plates to minimize coil-to-plate coupling [10]. Pre-programmed square wave (dc) and low frequency (20–60 Hz) $n = 1$ standing wave magnetic fields were applied to the plasma clearly generating RFA and at sufficiently large field amplitude caused RWM destabilization. The measured $n = 1$ RFA gain, defined as the ratio of the $n = 1$ plasma field amplitude to the applied vaccum field amplitude measured at the sensor, increases with β_N above the $n = 1$ no-wall β_N limit (figure 10). The result is similar to that found in DIII-D [27] using the same definition of the $n = 1$ RFA gain. One difference in the NSTX result is that the magnitude of the plasma response is measured using the RWM B_p sensors, rather than B_r sensors as done in DIII-D. The B_p sensors offer a greater signal to noise ratio, since the response of the B_r sensor signals in NSTX are curtailed by the influence of the passive stabilizing plates. While $n > 1$ unstable RWMs have been observed, the stable RFA generated from the applied $n = 1$ field and measured during periods of RWM stability is also observed to have $n = 1$.

A correlation between the frequency of ac components of the equilibrium field and the RWM in high beta, low q plasmas has been observed. This correlation is possibly due to interaction of the mode with ac error fields from the equilibrium coil systems or stabilizing plate eddy currents. The phenomenon has similarities to the dynamics theoretically explained by the F–A model of the mode matching frequency with the ac error field as the mode becomes unstable. The effect is shown in figure 11 with β_t decreasing from a maximum of 34% during 15 kHz, $n = 1$ tearing mode activity. The toroidal rotation is below the critical profile for RWM stabilization, $\omega_\phi/\omega_A(q) < 1/(4q^2)$, over the entire pulse duration. As the mode rotates and grows, it matches frequency at 385 Hz with the power supply ripple observed on several shaping coils (PF2 coil current is shown). The dynamics of the measured amplitude and phase closely resemble the F–A model results published in [15], figures 8 and 10. Initially, the $n = 1$ mode phase oscillates about some angle and eventually begins to rotate. The rotating mode phase velocity is not constant, also in agreement with the theory ([15], figure 10 frame (3,4)). Similarly to the RWM in figure 3(b), the phase velocity changes as the mode phase approaches then traverses the toroidal position of maximum intrinsic error field. However, in this case, the mode phase propagation is apparently *counter* to the direction of plasma rotation. It is interesting to note that in the F–A theory, a branch of the kink mode exists that also propagates counter to the direction of plasma rotation; however in the theory, this branch of the dispersion relation is always stable [14]. The $n = 1$–3 modes have similar peak amplitudes during the rotating period, but the $n = 2$ phase has different dynamics than the $n = 1$ mode, with slower toroidal rotation. Comparison of the difference between two opposing B_p sensors, ΔB_p, and the decomposed $n = 1$–3 mode amplitudes shows that the $n = 2$, 3 modes comprise a significant fraction of the total signal. The $n = 3$ mode has the largest amplitude at times near the $n = 1$ peak amplitude, but the $n = 2$ mode does not always follow this relationship. The local maxima of the $n = 1$ amplitude appear skewed or flattened compared with the total ΔB_p due to the significant $n = 2$ and 3 RWM components. Note that higher frequency $n = 1$ and 2 rotating modes with frequencies of 15 kHz and 30 kHz, respectively, are measured by magnetic pickup coils in this discharge, but they are easily distinguishable from the RWMs by their greatly disparate frequencies.

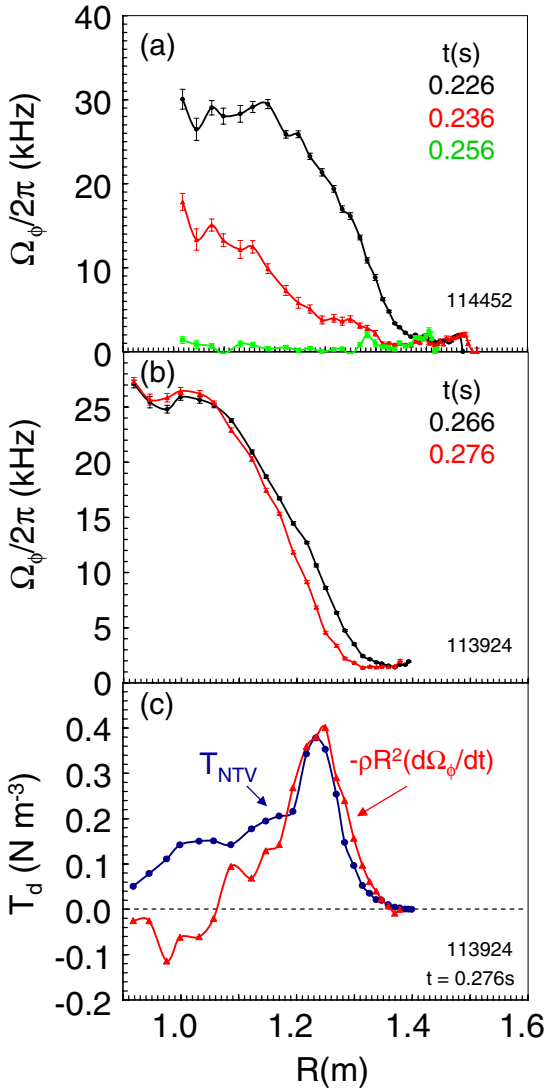

Figure 8. Plasma rotation damping during RWM (frames (*a*) and (*b*)) and the theoretical NTV damping torque profile (scaled) versus the measured plasma rotation damping at the onset of RWM growth (frame (*c*)).

6. Plasma rotation and equilibrium reconstruction

The importance of rotation in altering the high beta equilibrium has become apparent in discharges heated by intense co-injected neutral beams. Maximum core toroidal rotation frequencies $\omega_\phi/\omega_A = 0.48$ have been measured. NSTX EFIT reconstructions can now include measured thermal ion pressure and toroidal rotation, v_ϕ, profiles. The reconstruction considers currents in the vacuum vessel, passive stabilizing plates and other conducting structure as described in [5]. Both electron and ion thermal pressures are measured and are included in the reconstructions. An estimate of the fast ion pressure is included, using an ensemble of results from the TRANSP code. This estimate is assigned a large error bar to allow the reconstruction greater flexibility in fitting the total pressure profile. The profiles are input in real space and the full solution to the Bernoulli equation is used [29]. The Grad–Shafranov equilibrium equation remains the same, with the exception that the total plasma pressure, p_t, is considered to be

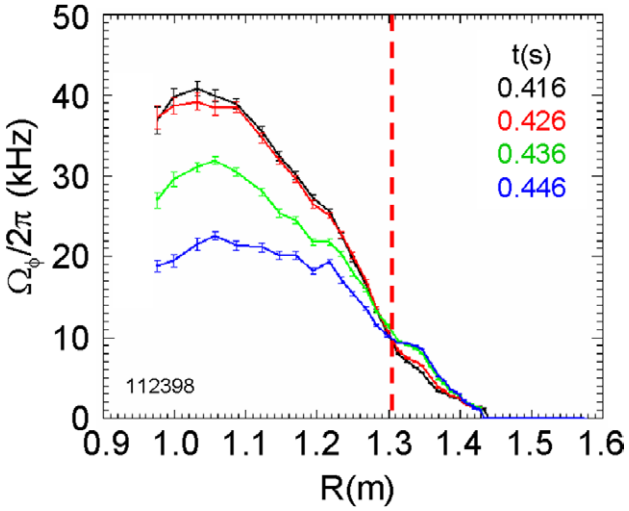

Figure 9. Rotation damping caused by an $n = 1$ tearing mode, showing clear outward momentum transfer.

both a function of the poloidal flux, ψ, and the major radius, R. With the condition that magnetic flux surfaces are isotherms, the Bernoulli equation can be integrated analytically [30], yielding the form

$$p_t(R, \psi) = p_s(\psi) \exp\left(\frac{p_\omega(\psi)}{p_s(\psi)} \frac{(R^2 - R_s^2)}{R_s^2}\right) \qquad (1)$$

for the total plasma pressure. Here, $p_w(\psi)$ and $p_s(\psi)$ are flux functions describing the measured plasma dynamic pressure in real space, $p_d = 1/2\rho v_\phi^2$, and the 'static' plasma pressure, respectively. Neither $p_w(\psi)$ nor $p_s(\psi)$ is directly measured. However, it can be shown that if the measured plasma kinetic pressure and dynamic pressure are both measured along the plasma midplane, both $p_w(\psi)$ and $p_s(\psi)$ can be defined analytically, including error bars transformed from the measured quantities, without the need for further computation or mapping. Since these measurements are taken at the plasma midplane on NSTX, $p_w(\psi)$ and $p_s(\psi)$ and their errors are defined and directly input to NSTX EFIT. Note that R_s is a constant of integration. However, while the specification of R_s is arbitrary, the ratio $p_w(\psi)/p_s(\psi)$ as defined by the measurements eliminates the dependence of $p_t(R, \psi)$ on R_s.

In addition to the rotational pressure constraint, topological flux surface constraints [29, 31] are imposed. The poloidal flux contours are constrained to be electron temperature, T_e, isotherms using measured values from the midplane Thomson scattering diagnostic. This constraint is required to maintain consistency with the magnetic flux surface isotherm assumption made in deriving the Bernoulli equation solution. The reconstruction quality is improved by the expanded physics model and flux isotherm constraints. Discharges with high v_ϕ (figure 12(*a*)) exhibit a clear outward shift of total pressure (white contours) from magnetic flux surfaces (black contours) in the plasma core. Peak pressure shifts of 18% of the minor radius from the magnetic axis have been reconstructed. The fitted plasma dynamic pressure is typically more peaked than the total pressure (figures 12(*c*) and (*b*)). Note that the measured total pressure, P_t is defined to be a sum of electron, ion, and fast particle pressures ($P_{e,i,f}$,

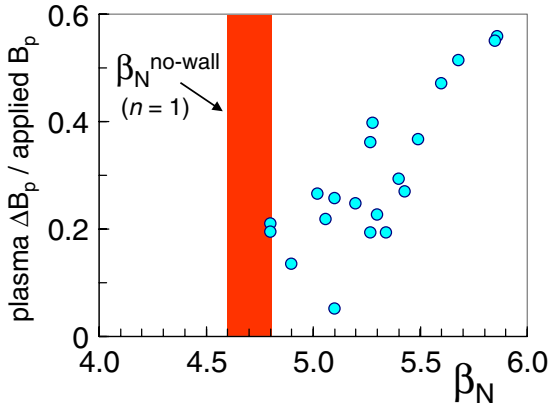

Figure 10. $n = 1$ resonant field amplification versus β_N for an externally applied $n = 1$ magnetic field.

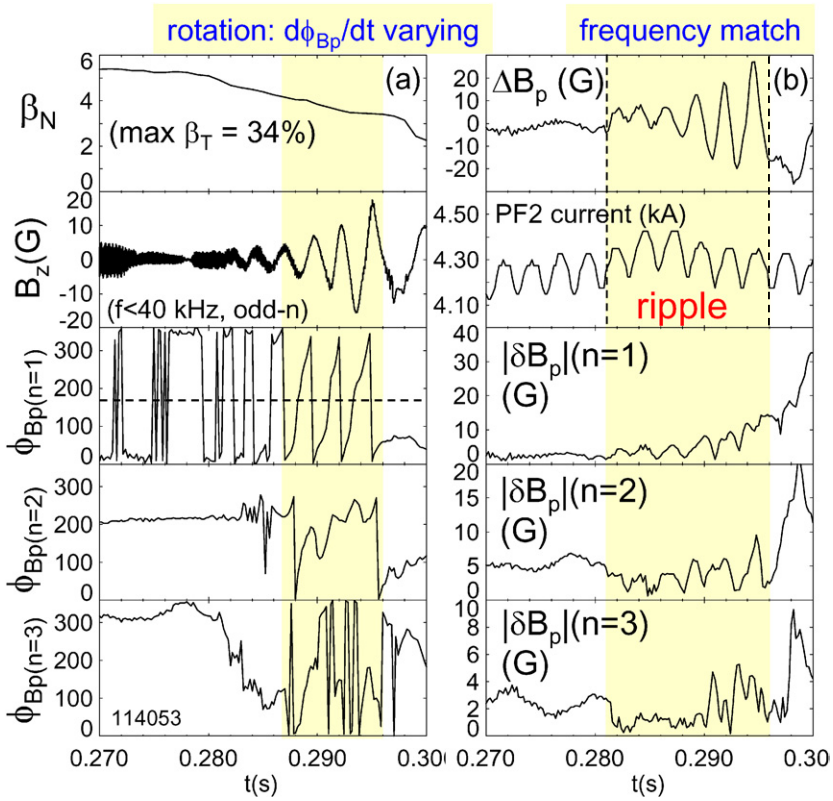

Figure 11. RWM evolution for mode with apparent phase lock to external field at 385 Hz. Column (*a*) shows the β_N and integrated B_z evolution, along with the computed phase, B_p, for $n = 1$–3 components analysed from the RWM B_p sensor array. Column (*b*) shows the evolution of the measured B_p field difference between diametrically opposed coil pairs, the shaping coil current showing the 385 Hz ripple and the amplitude of $n = 1$–3 components of the mode.

respectively). To allow a rapid, yet accurate, processing of full discharge reconstructions, a simple model of P_f is used and is assigned a large (50–100%) error bar. This approach allows greater breadth and detail in the fitted form of the total pressure profile. Also, at radial positions where P_i measurements are not available, simple assumptions for P_i are made, with large error assigned. This 'partial kinetic' prescription of P_t in the fitting procedure has been used successfully in static NSTX reconstructions and is used routinely [8]. The reconstructions typically have excellent fits to the flux isotherm constraint (figure 12(*d*); note that error bars are plotted at each R position on the plot) unless large non-axisymmetric MHD modes, such as the 1/1 internal mode, are present. This is understandable, as toroidal axisymmetry is assumed in the reconstruction procedure. The computed q in the central region of the plasma is also seen to decrease in time compared with static, high poloidal beta reconstructions, where q_0 does not decrease in time. This downward trend in q_0 is confirmed by initial reconstructions using internal magnetic pitch angle data from the motional Stark effect diagnostic.

These results provide initial insight on the potential alteration of plasma stability and Ω_{crit} calculations and offer input for future computation of stability with rotation. The computed stability of modes localized to the plasma edge, such

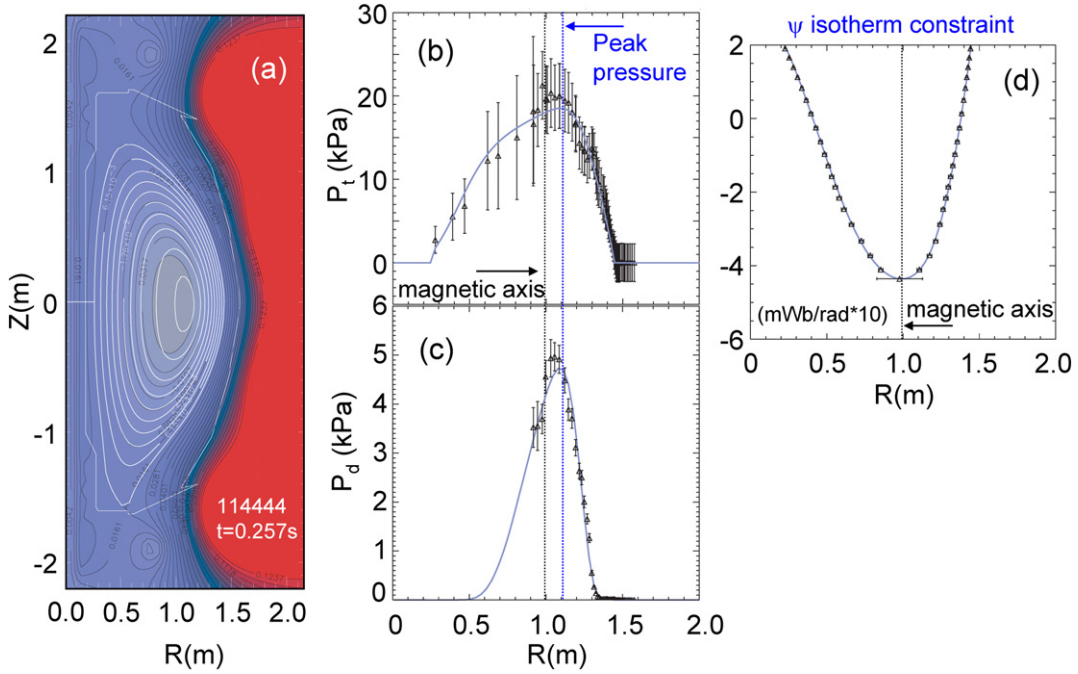

Figure 12. NSTX EFIT equilibrium reconstruction including toroidal rotation and flux isotherm constraints.

as high-n ballooning modes, will be unaffected by the inclusion of rotation, since the edge region is only slowly rotating, and the self-consistent equilibrium alteration is small in this region. The stability of global and core MHD modes can be affected in several ways by equilibrium variations due to plasma rotation. The downward evolution of q_0 observed will tend to reduce the ideal no-wall beta limit. For the majority of plasmas, that have monotonically increasing q profiles, the large outward shift of the peak pressure in relation to the magnetic axis moves the position of maximum pressure gradient into a region of larger q profile shear. This will generally increase mode stability. The rotation itself tends to be stabilizing. Future research is needed to make a thorough assessment of the influence on equilibrium alteration due to plasma rotation by performing self-consistent stability calculations that include the rotating equilibrium as input.

7. Summary and conclusions

High beta plasmas with normalized beta greater than the computed $n = 1$ ideal MHD no-wall stability boundary are routinely generated in NSTX for durations significantly longer than the conducting wall eddy current decay time as long as the plasma rotation is sufficiently large. We conclude that low-n global kink/ballooning modes are stabilized in these plasmas by the plasma rotation in the presence of a conducting wall. Reaching values of $\beta_N > \beta_{\text{Nno-wall}}$ does not rely on reduction of $\beta_{\text{Nno-wall}}$ by operating discharges with reduced no-wall beta limits by increasing pressure peaking or by other means. In fact, the no-wall stability boundary is typically surpassed in plasmas with low pressure peaking factors $\sim$2 and represent the highest β_N achieved in the device. The entire database, including wall-stabilized plasmas, shows no strong dependence of the maximum β_N as a function of l_i over the entire range of l_i operated, although such a correlation may exist over a limited range of l_i. High ratios of $\beta_N/l_i = 11$ have been reached.

As might be expected from experience in tokamaks of higher aspect ratio, unstable RWMs are observed when $\beta_N > \beta_{\text{Nno-wall}}$ and $\omega_\phi < \Omega_{\text{crit}}$. However, unlike higher aspect ratio tokamaks which have observed $n = 1$ RWMs to date, unstable RWMs with n up to 3 have been observed for the first time in recent NSTX experiments. The modes have been measured to rotate in certain cases before growing and causing significant plasma rotation damping and discharge termination. Measured mode rotation speeds have been of one to a few hundred hertz, of order $1/\tau_w$, which is significantly slower than the typical edge plasma rotation speed of one to a few kilohertz. The mode can have global extent and theoretically displays a strong ballooning character.

The critical plasma rotation frequency for RWM stabilization is considered a function of q, and a profile rather than a scalar at a specific q value. The theoretical scaling of Bondeson and Chu, $\Omega_{\text{crit}} = \omega_A/(Cq^2)$ with $C = 4$, well describes the stability criterion along with static ideal MHD stability calculation. As the measured non-axisymmetric field perturbation due to the RWM grows, the plasma rotation profile decreases rapidly and in a self-similar fashion, typically maintaining significant edge plasma rotation. This is consistent with the theory of damping due to NTV. The evolution of the plasma rotation profile during the damping is characteristically different from that observed due to tearing modes, which typically shows a strong outward momentum transfer. An initial investigation of the plasma response to applied non-axisymmetric fields ($n = 1$ dc and standing waves) was conducted, and the plasma response clearly increases with increasing β_N, a result also found in DIII-D.

The large plasma rotation of NSTX neutral beam heated plasmas can generate significant rotation effects on the

plasma equilibrium. These effects are increased by the low aspect ratio of the device. In general, contours of constant plasma pressure significantly separate from contours of poloidal magnetic flux in the plasma core where rotation is largest. This effect is incorporated into reconstructions of the plasma equilibrium including the dynamic pressure due to the measured plasma rotation as a constraint. Poloidal flux surfaces are also constrained to be electron temperature isotherms using measured T_e along the midplane. These equilibria will provide inputs for future stability calculations including plasma rotation.

Acknowledgments

This research was supported by the US Department of Energy under contracts DE-FG02-99ER54524 and DE-AC02-76CH03073.

References

[1] Ono M. *et al* 2000 *Nucl. Fusion* **40** 557
[2] Kaye S.M. *et al* 2005 *Nucl. Fusion* **45** S168
[3] Callen J.D. *et al* 1999 *Phys. Plasmas* **6** 2963
[4] Garofalo A.M. *et al* 2002 *Phys. Rev. Lett.* **89** 235001-1
[5] Sabbagh S.A. *et al* 2001 *Nucl. Fusion* **41** 1601
[6] Bondeson A. and Ward D.J. 1994 *Phys. Rev. Lett.* **72** 2709
[7] Garofalo A.M. *et al* 1999 *Phys. Rev. Lett.* **82** 3811
[8] Sabbagh S.A. *et al* 2002 *Phys. Plasmas* **9** 2085
[9] Menard J.M. *et al* 2005 *Nucl. Fusion* **45** 539
[10] Sabbagh S.A. *et al* 2004 *Nucl. Fusion* **44** 560
[11] Garofalo A.M. *et al* 2002 *Phys. Plasmas* **9** 1997
[12] Okabayashi M. *et al* 2001 *Phys. Plasmas* **8** 2071
[13] Menard J.E. *et al* 1997 *Nucl. Fusion* **37** 595
[14] Fitzpatrick R. and Aydemir A. 1996 *Nucl. Fusion* **36** 11
[15] Fitzpatrick R. 2002 *Phys. Plasmas* **9** 3459
[16] Shilov M. *et al* 2004 *Phys. Plasmas* **11** 2573
[17] Howl W. *et al* 1992 *Phys. Fluids* B **4** 1724
[18] Glasser A.H. and Chance M.C. 1997 *Bull. Am. Phys. Soc.* **42** 1848
Newcomb W. 1960 *Ann. Phys.* **10** 232
[19] Lao L.L. *et al* 1985 *Nucl. Fusion* **25** 1611
[20] Menard J.E. *et al* 2003 *Nucl. Fusion* **43** 330
[21] Bondeson A. and Chu M.S. 1996 *Phys. Plasmas* **3** 3013
[22] Shaing K.C. 2004 *Phys. Plasmas* **11** 5525
[23] Fitzpatrick R. 1993 *Nucl. Fusion* **33** 1049
[24] Shaing K.C., Hirshman S.P. and Callen J.D. 1986 *Phys. Fluids* **29** 521
[25] Lazzaro E. *et al* 2002 *Phys. Plasmas* **9** 3906
[26] Boozer A.H. 2001 *Phys. Rev. Lett.* **86** 5059
[27] Garofalo A.M., Jensen T.H. and Strait E.J. 2003 *Phys. Plasmas* **10** 4776
[28] Bialek J.M. *et al* 2001 *Phys. Plasmas* **8** 2170
[29] Lao L.L. *et al* 2005 *Fusion Sci. Technol.* **48** 968
[30] Waelbroeck F.L. 1996 *Phys. Plasmas* **3** 1047
[31] Zhang C. and Lao L.L. 2005 Tokamak equilibrium reconstruction with topological and current hole constraints *General Atomics Report* A24582